Ocean Engineering 121 (2016) 516–529

Contents lists available at ScienceDirect

Ocean Engineering

journal homepage: www.elsevier.com/locate/oceaneng

A maximum capture width tracking controller for ocean wave energy converters in irregular waves

P. Hardy [a,*], B.S. Cazzolato [a,**], B. Ding [a], Z. Prime [b]

[a] The University of Adelaide, School of Mechanical Engineering, Adelaide, South Australia, Australia
[b] The University of New South Wales, School of Mechanical and Manufacturing Engineering, Sydney, New South Wales, Australia

ARTICLE INFO

Article history:
Received 25 January 2016
Received in revised form
19 April 2016
Accepted 30 May 2016

Keywords:
Oscillating water column
Wave energy converter
Latching control
Maximum power point tracking
Gradient-ascent
Model uncertainty
Irregular waves

ABSTRACT

A maximum capture width tracking (MCWT) controller for ocean wave energy converters is presented. The MCWT controller is a maximum power point tracking (MPPT) controller modified to account for incoming wave conditions as well as WEC power output. The MCWT controller will be applied to latching control of an oscillating water column with Wells turbine, optimising the latching time based on sea state. The performance of the proposed MCWT latching controller will be compared to that of an MPPT latching controller in both stationary and transitioning sea states. In stationary seas, it will be shown that both controllers can optimise capture width to within the bounds of certainty that the optimal capture width can be known for a WEC in stochastic waves. In transitioning seas, it will be shown that the MCWT controller is robust to a changing environment, whereas the MPPT controller is not.

1. Introduction

Ocean wave energy harvesting has been a popular area of research since the 1970s oil crisis (Cruz, 2008). However, despite over 40 years of effort, wave energy remains in the research and prototype stages, with only a few pilot plants connected to grid worldwide (Hughes and Heap, 2010). The challenge preventing commercialisation of ocean wave energy harvesting is the efficient conversion of the highly variable broadband wave energy resource to grid frequency electricity. Feedback controlled oscillating systems have been a popular solution to this power conversion problem due to their versatility and ease of deployment (Lattanzio and Scruggs, 2011), with heaving buoys and oscillating water columns (OWCs) both receiving considerable attention over the years.

A feedback control strategy for oscillating wave energy converters (WECs) that has received considerable research attention over the years is latching. Latching is a passive, non-linear control method which attempts to achieve optimum phase between the excitation force and wave energy converter velocity, therefore maximising real power, by fixing the motion of the WEC during parts of the cycle (Clément and Babarit, 2012). Latching has been used to control the natural period of a WEC heaving in regular waves (Clément and Babarit, 2012; Babarit and Clément, 2006; Babarit et al., 2004), where power absorption was found to increase for sub-resonant and post-resonant frequencies when the natural period was controlled to be equal to the incident wave period, and three times the incident wave period, respectively. Optimal latching times for the 4-DoF SEAREV device were derived using Pontryagin's maximum principle (Babarit and Clément, 2006), resulting in performance increasing by a factor of two in simulated ocean waves compared to the uncontrolled system. Small scale experiments involving an OWC with a simple threshold latching controller found that latching increased the efficiency in irregular waves by 200–350% compared to the uncontrolled case (Lopes et al., 2009).

Optimal latching of a floating spar-buoy OWC with bi-radial turbine was studied in Henriques et al. (2016) considering full scale air compressibility. The optimal latching controller was implemented using a receding horizon formulation, where the optimal latching and unlatching times over a future time-period, or horizon, were determined using Pontryagin's maximum principle considering exact knowledge of the excitation force time-series over the future horizon. Simulations of the optimally latched WEC in irregular waves found that latching could significantly increase capture width if the controller horizon exceeded the energy period of the sea state, however, for shorter horizons, the optimal latching controller was found to be less effective than a fixed passive damping. In reality, this means that for optimal latching to be

* Principal corresponding author.
** Corresponding author.
E-mail addresses: peter.hardy@adelaide.edu.au (P. Hardy), benjamin.cazzolato.@adelaide.edu.au (B.S. Cazzolato).

http://dx.doi.org/10.1016/j.oceaneng.2016.05.045
0029-8018/

effective, the WEC exciting force time-series must be predicted accurately over a horizon at least as long as the energy period of the sea state. In Ringwood (2012) it was found that the exciting force could be predicted accurately, quantified as less than 40% error, approximately 0.5–1 wave periods into the future depending on the bandwidth of the sea state, which is shorter than the energy period and insufficient for optimal latching control. In general, WEC controllers which maximise power on a wave-by-wave basis are not currently feasible due to the requirement for accurate prediction of incoming waves (Babarit et al., 2012). Hence, whilst latching can significantly improve the performance of a WEC, optimisation is difficult due to the need for future wave information and an optimal latching control strategy has yet to be implemented in the real world (Clément and Babarit, 2012).

Motivated by the difficulty of wave prediction, non-model based adaptive controllers have been developed which optimise WEC power take-off (PTO) parameters based on the current sea state. Adaptive control schemes of extremum seeking control and maximum power point tracking have been applied to WECs. Adaptive controllers, colloquially referred to as "perturb and observe", work in the WEC power extraction sense by slightly altering an aspect of the PTO, such as the spring stiffness or damping, determining if the perturbation caused the extracted power to increase, and continually perturbing in an attempt to find the point of maximum power. Extremum seeking control was investigated in Hals et al. (2011) to optimise PTO damping for a heaving WEC with constrained motion in non-stationary sea states. The extremum seeking controller yielded better performance for the non-linear WEC than a gain scheduled damping controller, however, as an optimal damping profile for the non-stationary sea state was not given, it is unknown how damping produced by the controller compared to optimal. Extremum seeking control was used to maximise extracted power in a simulated heaving WEC in stationary irregular waves (Garcia-Ross et al., 2012), with the controller found to perform effectively for both linear and nonlinear PTO. The extremum seeking controller in Garcia-Ross et al. (2012) was truly model independent, unlike (Hals et al., 2011) which required estimates of the instantaneous exciting force, however, the efficacy of this model independent controller in non-stationary sea states is yet to be verified.

Maximum power point tracking (MPPT), a gradient-ascent type method commonly used in wind and solar energy converters, has been investigated for adaptive PTO control in a WEC (Amon et al., 2009, 2012), where the load resistance of a linear generator was tuned by varying the duty cycle of a buck converter. The investigation considered a surface following WEC, effectively neglecting hydrodynamics, and focused on the effects of varying the update rate and step size of the MPPT algorithm on the average power output for a single sea state. It was concluded that MPPT could significantly improve average power output in stationary irregular waves. Real ocean waves, however, are not stationary, and MPPT algorithms are known to become confused in changing environmental conditions as the controller cannot determine the cause of a change in measured output power (Abdullah et al., 2012; Kazmi et al., 2010, 2011). MPPT controllers which are robust to environmental changes have been developed for wind turbines (Kazmi et al., 2011) by combining wind speed measurements, to detect changes in the environment, with output power measurements to determine if the maximum power point had been reached.

A similar control algorithm to Kazmi et al. (2011) has been applied to a WEC by measuring incoming wave power in addition to WEC power to track the maximum capture width (Ding et al., 2015). The maximum capture width tracking algorithm (MCWT) was used to control PTO damping for a heaving, submerged WEC in irregular waves. MCWT was found to drive PTO damping towards optimal in both stationary and transitioning sea states, however, the damping was then found to oscillate randomly about optimal. It was explained that the gradient-ascent type controller became ineffective when the sensitivity of the capture width to damping change was less than the variance of the capture width estimate, which occurred when the slope of the power vs. damping characteristic was shallow. Hence, it was shown that MCWT could optimise damping to within some bounds dependent on WEC dynamics.

This work will expand on Ding et al. (2015) by investigating the performance of MPPT and MCWT latching control of an OWC in irregular waves. MPPT/MCWT latching controllers will be used to optimise the latching time of an OWC with Wells turbine in both stationary and transitioning sea states. A mathematical model of an OWC with Wells turbine will be presented in Section 2, followed by details of the MPPT/MCWT algorithms in Section 3, and simulation methods in Section 4. Results of Monte-Carlo simulations will be used in Section 5.1 to determine confidence intervals for the capture width estimate and optimisation bounds for the latching time, before results of MPPT/MCWT latching control simulations are presented in Section 5.3. The MPPT/MCWT latching control results will show that in stationary sea states both latching controllers can optimise capture width to within the confidence bounds that the optimal capture width can be known. In transitioning sea states it will be shown that MCWT control is superior to MPPT. Finally, a brief investigation into OWC performance in bi-modal waves will be performed, where it will be concluded that MCWT latching control can be effective in bi-modal seas.

2. Mathematical model

Hydrodynamic models of wave energy converters (WECs) are typically estimated based on linear wave theory, which is a good approximation for WECs operating in waves of moderate amplitude. The assumption of linearity allows for the net flux through the turbine to be considered as the sum of separate scattering and radiation fluxes (Evans, 1982);

$$\begin{aligned} Q^T(\omega) &= Q^S(\omega) - Q^R(\omega) \\ &= \eta(\omega) q^S(\omega) - \frac{i\omega p_c}{\rho g} q^R(\omega) \end{aligned} \tag{2.1}$$

where $Q^T(\omega)$ is the net flow of water into the OWC chamber, $Q^S(\omega)$ and $Q^R(\omega)$ the net scattering and radiation fluxes respectively, η the incoming wave amplitude, ω the wave frequency, ρ is the water density, g is gravitational acceleration, p_c is the air pressure inside the OWC chamber, $q^S(\omega)$ is the scattering flux induced by a wave of unity amplitude and $q^R(\omega)$ the radiation flux induced by unity amplitude air pressure oscillation. Furthermore, the radiation can be decomposed into real and imaginary parts (Evans, 1982);

$$-\frac{i\omega p_c}{\rho g} q^R(\omega) = \left[B(\omega) - iA(\omega) \right] p_c \tag{2.2}$$

where $B(\omega)$ and $A(\omega)$, defined as the radiation conductance and susceptance respectively (Falnes, 2002), are real, frequency dependent quantities analogous to damping and added mass respectively in a rigid body system (Evans and Porter, 1995).

A two-dimensional OWC was considered, a schematic of which is shown in Fig. 1. The scattering and radiation flux problems for the OWC were solved at discrete frequencies using a Galerkin approximation (Evans and Porter, 1995), considering 500 evanescent modes and five Chebyshev polynomial test functions to represent the velocity of each mode. The radiation flux transfer function, $H^R(\omega) = B(\omega) - iA(\omega)$, was identified using a least

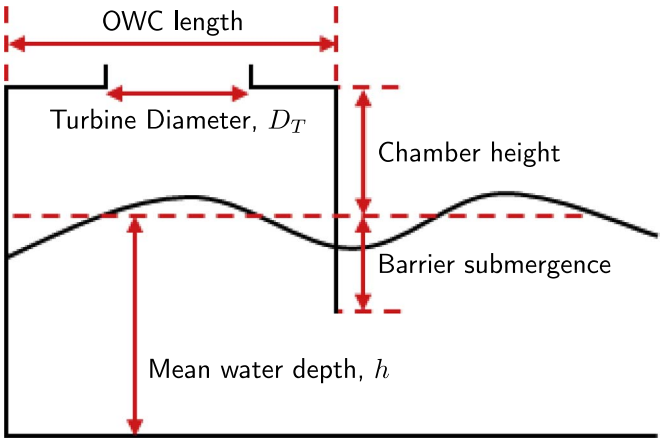

Fig. 1. OWC schematic.

squares approximation (Perez and Fossen, 2009), where it was found that a 4th order model provided a good fit to the radiation flux data from the Galerkin solution. The frequency response of the identified radiation model is shown in Fig. 2 along with the radiation flux data. The radiation flux transfer function is represented in control canonical state space form as:

$$\left[\begin{array}{c|c} A^R & B^R \\ \hline C^R & D^R \end{array}\right] = \left[\begin{array}{cccc|c} -1.789 & -2.106 & -1.152 & -0.6939 & 1 \\ 1 & 0 & 0 & 0 & 0 \\ 0 & 1 & 0 & 0 & 0 \\ 0 & 0 & 1 & 0 & 0 \\ \hline 4.243^{-4} & 6.714^{-4} & 7.055^{-4} & 0 & 0 \end{array}\right] \tag{2.3}$$

Considering OWC chamber pressure as the input to the radiation model, the instantaneous radiation flux in the time-domain is given by

$$Q^R(t) = C^R e^{A^R(t-t_0)} z^R(t_0) + C^R \int_{t_0}^{t} e^{A^R(t-\tau)} B^R p_c(\tau) d\tau + D^R(t), \tag{2.4}$$

where $z^R(t)$ is the state vector of the radiation flux model and t_0 is the initial time for state space equation solutions (Taghipour et al., 2008; Yu and Falnes, 1995). In this work $t_0 = 0$ and $z^R(t_0) = 0$.

The scattering flux transfer function was identified using a least squares approximation, where a 6th order model was found to provide an acceptable fit to the scattering flux data from the Galerkin solution. The frequency response of the identified scattering model is shown in Fig. 2 along with the scattering flux data. The magnitude of the scattering flux model agrees well with the scattering data for wave periods longer than 5 s, below which the fit becomes poor due to the presence of a secondary, sloshing resonance. This model error is acceptable as waves of such short period are not useful for energy extraction and the induced scattering flux is negligible compared with that of longer period waves. The scattering flux transfer function is represented in control canonical form as

$$\left[\begin{array}{c|c} A^S & B^S \\ \hline C^S & D^S \end{array}\right] = \left[\begin{array}{cccccc|c} -2.947 & -4.674 & -4.553 & -3.172 & -1.436 & -0.3895 & 1 \\ 1 & 0 & 0 & 0 & 0 & 0 & 0 \\ 0 & 1 & 0 & 0 & 0 & 0 & 0 \\ 0 & 0 & 1 & 0 & 0 & 0 & 0 \\ 0 & 0 & 0 & 1 & 0 & 0 & 0 \\ 0 & 0 & 0 & 0 & 1 & 0 & 0 \\ \hline 0 & 0 & 1.940 & 7.465^{-2} & 7.436 & -2.852^{-3} & 0 \end{array}\right] \tag{2.5}$$

Considering incoming wave elevation as the input to the scattering flux model, the instantaneous scattering flux in the time-domain is given by

$$Q^S(t) = C^S e^{A^S(t-t_0)} z^S(t_0) + C^S \int_0^t e^{A^S(t-\tau)} B^S \eta(\tau) d\tau + D^S(t), \tag{2.6}$$

where $z^S(t)$ is the state vector of the scattering flux model and $z^S(t_0) = 0$.

The expansion/compression of air in the chamber and passage of air through the turbine are assumed to be isentropic and adiabatic processes. The air pressure inside the OWC chamber, assuming that air is an ideal gas, is given by

$$p_c = \frac{m_c R T_c}{V_c}, \tag{2.7}$$

where T_c, m_c and V_c are instantaneous air temperature, air mass and air volume inside the OWC chamber respectively, and R is the universal gas constant. The air temperature inside the OWC chamber can be found from the first law of thermodynamics considering the air chamber as a control volume with single inlet/outlet through the turbine (Gkikas and Athanassoulis, 2014);

$$\frac{dT_c}{dt} = -\frac{p_c}{m_c c_v}\frac{dV_c}{dt} + \frac{1}{m_c}\frac{dm_c}{dt}\left(\frac{c_p}{c_v}\max\left(T_c,\ T_{atm}\right) - T_c\right), \tag{2.8}$$

where c_v and c_p are the specific heats of air under constant volume and constant pressure processes respectively. The volume of air in the OWC chamber is given by

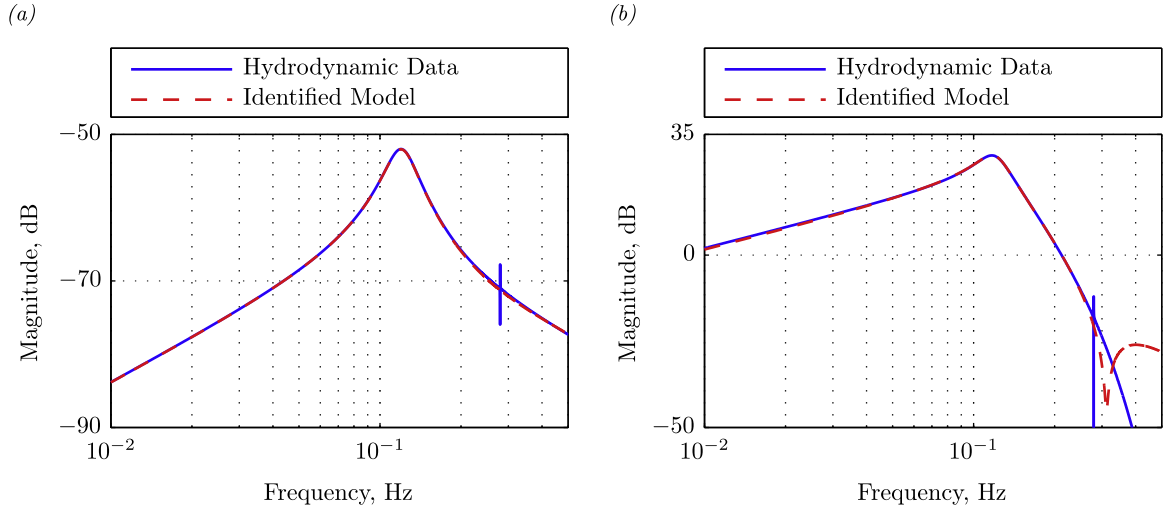

Fig. 2. Magnitude of identified (a) radiation flux and (b) scattering flux models compared with hydrodynamic data from the Galerkin solution.

$$V_c(t) = V_0 - \mathrm{Re}\left(\frac{Q^T(\omega)e^{i\omega t}}{i\omega}\right), \tag{2.9}$$

where V_0 is the mean volume of the air chamber and Re indicates that only the real part of the phasor is considered.

A standard Wells turbine was included in the model for power take-off. The mass flow rate of air passing through the turbine is (Falcao and Justino, 1999)

$$\frac{dm_c}{dt} = p_c\left(\frac{K_T D_T}{N_T}\right), \tag{2.10}$$

where K_T is a constant dependent on turbine geometry but independent of turbine size, D_T is the turbine diameter and N_T is the turbine rotational speed in rad/s. Turbine rotational speed must be limited to prevent formation of shock waves inside the turbine, which occurs when the blade tip speed approaches the speed of sound. The maximum turbine rotational speed is given by Falcão and Rodrigues (2002)

$$N_T \le \frac{2c_a \mathrm{Ma}}{D_T} \tag{2.11}$$

where c_a is the speed of sound in air at atmospheric conditions and Ma is the Mach number of the blade tip speed, typically restricted to Ma = 0.6. Mechanical power output from the Wells turbine is determined using dimensionless experimental turbine data relating differential air pressure to turbine power. The non-dimensionalised experimental data, shown in Fig. 3, was obtained from Falcão and Justino (1999), with dimensionless pressure ψ and power Π given by

$$\psi = \frac{p_c}{\rho_a N_T^2 D_T^2} \tag{2.12}$$

$$\Pi = \frac{P_{in}}{\rho_a N_T^3 D_T^5} \tag{2.13}$$

where P_{in} is the instantaneous turbine power and ρ_a is the density of the air passing through the turbine. As airflow is bi-directional

$$\rho_a = \max\left(\frac{m_c}{V_c},\ \rho_{atm}\right) \tag{2.14}$$

where ρ_{atm} is atmospheric air density; $\rho_{atm} = P_{atm}/RT_{atm}$.

Latching control is implemented in the model by adding a latching variable $\delta_L \in [0, 1]$ to Eq. (2.10)

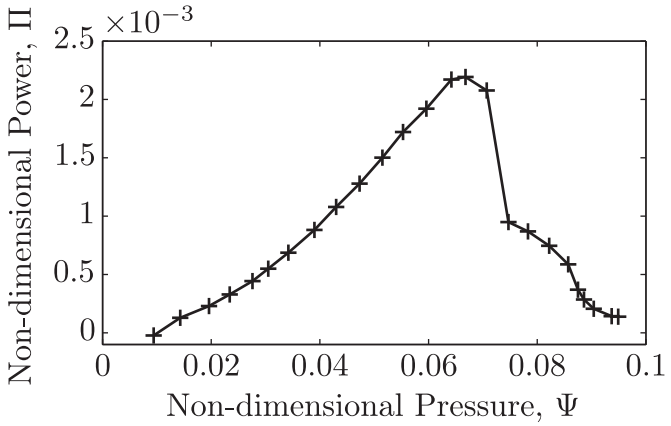

Fig. 3. Non-dimensional pressure ψ vs. power Π characteristic for Wells Turbine. Data obtained from Falcão and Justino (1999). Discrete values used in look-up table indicated by +, interpolated values indicated by solid line.

$$\frac{dm_c}{dt} = \delta_L p_c\left(\frac{K_T D_T}{N_T}\right) \tag{2.15}$$

where $\delta_L = 0$ and $\delta_L = 1$ indicate the system is latched and unlatched respectively. Similarly, the dimensionless turbine power is also modified to

$$\Pi = \delta_L \frac{P_{in}}{\rho_a N_T^3 D_T^5}. \tag{2.16}$$

The mean efficiency of the OWC, or relative capture width, is given by

$$CW = \frac{P}{J} \tag{2.17}$$

where P is the mean turbine power and J the incident wave power;

$$J = W\int_0^\infty \frac{2\rho g^2 D(kh)}{4\omega} S(\omega)d\omega \tag{2.18}$$

with W the OWC width, $S(\omega)$ the incident wave spectra and $D(kh)$ the depth function (Falnes, 2002)

$$D(kh) = \left(1 + \frac{2kh}{\sinh(2kh)}\right)\tanh(kh) \tag{2.19}$$

which is a function of wavenumber k and water depth h.

3. Maximum power point/capture width tracking algorithms

Maximum power point tracking (MPPT) is a gradient-ascent type algorithm which maximises power with respect to a chosen variable, in this case latching time. MPPT works by continually perturbing one or more system variables and observing the associated change in power, the goal being to perturb such that power increases. For MPPT to be effective the power vs. perturbed variable curve, $P = f(x)$, should be convex with a well defined global maxima occurring at x_{opt}, as then MPPT will continually perturb x such that $x \to x_{opt}$, increasing and ideally maximising power.

The MPPT algorithm used to increase WEC power by perturbing the latching time is

$$T_{L,\,k+1} = \left| T_{L,\,k} + \mu\ \mathrm{sgn}\left(\frac{\hat{P}_k - \hat{P}_{k-1}}{T_{L,\,k} - T_{L,\,k-1}}\right)\right|, \tag{3.1}$$

which is a discrete time algorithm where $T_{L,\,k}$ is the latching time at sample k, $\hat{P}_k$ is the estimate of the mean OWC power output at sample k, μ is the latching time step size with dimensions of seconds, and 'sgn' is the signum function. The OWC latches when the chamber pressure becomes equal to atmospheric, then MPPT will determine the time interval for which the OWC will remain latched.

The proposed maximum capture width tracking (MCWT) latching control algorithm is

$$T_{L,\,k+1} = \left| T_{L,\,k} + \mu\ \mathrm{sgn}\left(\frac{C\hat{W}_k - C\hat{W}_{k-1}}{T_{L,\,k} - T_{L,\,k-1}}\right)\right|, \tag{3.2}$$

where $C\hat{W}_k$ is the estimate of the mean OWC capture width at sample k.

Both the discrete MPPT and MCWT algorithms have two independent degrees of freedom; the update rate and the step size (Amon et al., 2009, 2012). The update rate controls the rate at which the controller responds to changes in the mean power/capture width estimate, and hence changes in incident wave conditions. A fast update rate is desirable for the controller to

respond quickly to changes in incident wave conditions, however, the update rate is also inversely proportional to the amount of new information used to influence the next controller action, and hence the variance in the power/capture width estimate. The step size μ controls the resolution of the MPPT/MCWT algorithm and determines how aggressively the controller responds to changes in the mean power/capture width output. Methods to determine optimal μ exist (Barzilai and Borwein, 1988; Yuan, 2008), however, such methods can be mathematically complex. Typically, selection of optimal parameters for gradient ascent type algorithms is a trial and error exercise (Snyder, 2000). A good trial and error approach is to simulate the controllers for a range of μ, increasing μ by an order of magnitude each simulation; $\mu_1 = 0.001$, $\mu_2 = 0.01$, etc. This will narrow the search for an optimal μ to within a decade and subsequent simulations for μ within this decade should yield a good choice of step size.

4. Modelling methods

Time-domain modelling was performed in Simulink using the inbuilt `ode45` solver, being a 5th order, variable step Runge–Kutta solver. A list of the simulation variables, including OWC and turbine dimensions, can be found in Table 1a.

The OWC was simulated in irregular waves considering conditions along the South Australian coast, a region with one of the highest wave energy densities in the world (Hughes and Heap, 2010). The OWC was simulated for wave conditions corresponding to the 10th, 50th and 90th percentile sea states occurring at Cape du Couedic, South Australia (Hemer and Griffin, 2010), listed in Table 1b as S_{10}, S_{50} and S_{90} respectively. Waves were generated from an ITTC spectra, being a fully developed spectra of Pierson-Moskowitz type (McCormick, 2010, p. 137; ITTC, 2002) as wave conditions along the South Australian coast can be categorised as fully developed uni-modal seas (Hemer and Griffin, 2010). Simulated sea spectra, S_w, each consisted of 1000 discrete frequencies initialised with random phase ϕ_r. Frequencies were randomised to prevent time-series repetition (Faltinsen, 1993, p. 26) by creating a uniformly discretised spectra with frequencies ω_i and resolution $\Delta\omega$, then offsetting each frequency by a small, random value; $\omega_r = \omega_i + \theta\frac{\Delta\omega}{2}$, where $\theta \in [-1, 1]$ is a uniformly distributed random variable. The wave elevation time series is then given by $s_w(t) = \sum_{r=1}^{1000} \sqrt{2S_w(\omega_r)\Delta\omega}\,\sin(\omega_r - \phi_r)$ where $\phi_r = \theta\pi$. Whilst wave elevation time series were randomised, all time series produced were repeatable. Random numbers used for frequency randomisation and random phase generation were generated by a Mersenne Twister random number generator initialised with a set seed value.

Table 1.
Parameters and sea states used for simulations.

(*a*) *Simulation parameters*

OWC/turbine dimension	Quantity	Simulation variable	Quantity
Front-to-rear barrier length	10 m	Atmospheric temperature, T_{atm}	300 K
Front barrier submergence	10 m	Atmospheric pressure, P_{atm}	101.3 kPa
Width to incoming waves, W	10 m	Universal gas constant, R	287.05 J kg^{-1} K^{-1}
Chamber height	10 m	Specific heat, c_v	717.5 J kg^{-1} K^{-1}
Water depth, h	20 m	Turbine power sample time, T_s	0.1 s
Turbine diameter, D_T	4 m	Wave amplitude sample time, T_w	0.5 s
Turbine speed, N_T	94.25 rad s^{-1}	Number of FFT points, N_F	128
Turbine constant, K_T	0.6803 (Falcao and Justino, 1999)	`ODE45` solver absolute and relative tolerances	1×10^{-3}

(*b*) *South Australian sea states* (Hemer and Griffin, 2010)

Sea state	Peak period T_p (s)	Significant wave height H_s (m)	Percentile
S_{10}	11.6	1.47	10
S_{50}	12.7	2.45	50
S_{90}	13.9	3.94	90

Dimensions of the OWC and turbine were chosen considering system performance in South Australian sea states. The design procedure for the OWC involved increasing dimensions until the resonant period was as close as possible to the period of peak energy content, $T_e = 0.858T_p$ (ITTC, 2002) where T_p is the peak period of the mean South Australian sea state. The OWC considered has a resonant period of 8.8 s, which is significantly different to the 10.9 s energy period of the 50th percentile sea state, as further increase in OWC dimensions lead to breakdown in the solid body model of the water column (Evans and Porter, 1995), causing sloshing inside the OWC. A large diameter turbine with high rotational speed was chosen to reduce the risk of aerodynamic stall, which occurs when the pressure differential across the turbine exceeds the critical value of $\psi = 0.067$ (Falcão, 2002), by reducing non-dimensional pressure according to Eq. (2.12). In reality, a smaller diameter turbine with by-pass valve to relieve chamber pressure, as in Falcao and Justino (1999), may be more appropriate, however, this is not considered in this investigation. Turbine speed was maintained constant at the maximum value, given by Eq. (2.11), for all simulations, which is desirable in a real life system to reduce the complexity of the power electronics that connect the generator to the electrical grid.

Instantaneous wave elevation samples were taken with a zero-order hold with sample time T_w. The continuous wave spectra $S(\omega)$ was estimated by taking the fast Fourier transform (FFT) of wave amplitude measurements, yielding the discrete frequency spectral estimate $\hat{S}(\omega)$. An estimate of the incoming wave power is then obtained from Eq. (2.18) by replacing the continuous integration by the sum of FFT frequencies and the integration variable $d\omega$ by the FFT frequency resolution $\Delta\omega = 2\pi F_w/N_F$, yielding

$$\hat{J} = \rho g^2 \frac{\pi F_w}{N_F} \sum_{i=1}^{N_F/2} \frac{D(k_i h)}{\omega_i} \hat{S}(\omega_i) \tag{4.1}$$

where $F_w = 1/T_w$ is the sample frequency of wave amplitude measurements and N_F is the number of FFT points, of which only the $N_F/2$ frequencies, i.e., below the Nyquist frequency, are considered. Low FFT resolution was adopted to increase the degrees of freedom of the spectral estimates $\hat{S}(\omega)$ through increasing the number of averages (Goda, 2010, p. 445; Bendat and Piersol, 2010, p. 281), reducing the variance of the wave power estimates $\hat{J}$. For the long times-series investigated in this work, multiple spectral measurements $\hat{S}(\omega)$ are combined using Welch's method of overlapped averages (Welch, 1967) to obtain a single spectra estimate for the time-series.

Mechanical power output from the Wells turbine was determined from a look-up table populated with non-dimensionalised experimental turbine data. Linear interpolation was used between discrete look-up table values, and outside of the data range the relationship between OWC pressure and turbine power was assumed constant. Instantaneous turbine power samples $P_w = \frac{1}{T_s}\int_0^{T_s} P_{in}(t)dt$ were taken using a zero-order hold with sample time T_s and stored in a buffer without overlap, with buffer length, n_{buf}, set corresponding to the desired update rate of the controller. An estimate of the mean turbine power for the sea state is then

determined by averaging the buffered turbine power samples, $\hat{P} = \frac{1}{n_{buf}} \sum_{i=1}^{n_{buf}} P_{w,i}$.

The latching controllers used in this work were programmed to latch the OWC when the chamber pressure became equal to atmospheric, which is the optimal latching condition for OWCs in sub-resonant waves (Jefferys and Whittaker, 1985), and unlatch after a time interval determined by the controller, designated the latching time. Latching variable changes were rate limited, meaning latching and unlatching did not occur instantaneously, rather the latching variable δ_L was ramped over 100 ms. Finally, as time cannot be negative, latching time was restricted to being positive.

5. Simulations

The maximum capture width tracking (MCWT) algorithm introduced in Eq. (3.2) attempts to maximise mean capture width for a sea state. The MCWT controller therefore requires knowledge of the mean capture width for the sea state, *CW*. In monochromatic waves the mean capture width can be determined exactly using Eq. (2.18). Real ocean waves, however, are random, and consequently the mean capture width can never be known exactly. Rather, mean capture width can only ever be estimated from a finite time-series with some level of certainty. The mean capture width estimate is given by

$$\hat{CW} = \frac{\hat{P}}{\hat{J}} \tag{5.1}$$

where $\hat{J}$ and $\hat{P}$ are finite-time estimates of the mean incoming wave power and the mean power produced by the WEC respectively. Confidence intervals for the mean capture width *CW*, being a region likely to contain *CW*, can be derived using a set of estimates $\hat{CW}$. Monte-Carlo simulations will be used in Section 5.1 to derive 95% confidence intervals for *CW* for the 10th, 50th and 90th percentile sea states, which will then be used to define latching time optimisation bounds for each state in Section 5.2. MPPT/MCWT latching control of an OWC will be investigated in Section 5.3.

5.1. Confidence bounds for capture width

Monte-Carlo simulations were performed for the latching controlled OWC in irregular waves to investigate the distribution, variance and mean of the capture width estimate $\hat{CW}$ to derive 95% confidence intervals for the mean capture width *CW*. Simulations were performed for the 10th, 50th and 90th percentile sea states listed in Table 1b where 250 unique time-series of 5 h length were used for each state. The latching time was fixed for each run, but over the course of the simulations was varied from 0 s to 2.5 s in 0.1 s increments, yielding 250 estimates $\hat{CW}$ of *CW* for each fixed latching time for each sea state. Results of $\hat{CW}$ vs. fixed latching time considering only the first 20 min of each 5 h time-series are shown in Fig. 4a for the 50th percentile sea state, where it is apparent that $\hat{CW}$ varies significantly between time-series. The large variance in $\hat{CW}$ determined over 20 min periods indicates that long measurement periods are needed to obtain an accurate estimate of *CW* for the sea state.

The distribution of $\hat{CW}$ was investigated for Gaussian behaviour by performing Chi-Square goodness-of-fit tests on the Monte-Carlo results with a significance level of 5%. Goodness-of-fit test results for the 50th percentile sea state are shown in Fig. 4b which indicate that for time-series lengths of at least 20 min the distribution of $\hat{CW}$ for a fixed latching time can be considered approximately Gaussian. A series of hypothesis rejections appear for the 180 min time-series, however, these rejections disappear with perturbation in time-series length, suggesting that non-Gaussian behaviour is occurring in the incoming wave time-series at this point, causing non-Gaussian behaviour of $\hat{CW}$. Goodness-of-fit results for the 10th and 90th percentile sea states are similar to those from the 50th percentile, indicating that $\hat{CW}$ for a fixed latching time can be approximated as Gaussian for time-series lengths of at least 20 min. No comment is made regarding the distribution of estimates obtained using shorter time-series lengths as this was not tested.

As the estimate $\hat{CW}$ for each fixed latching time can be regarded as Gaussian, confidence intervals for *CW* estimated from $\hat{CW}$ can be derived if *CW*, being the true mean of $\hat{CW}$, is known along with the variance σ_{CW}^2 of $\hat{CW}$. The mean capture width for each fixed latching time was taken as the mean of the 250 unique capture width estimates obtained from 5 h time-series. Whilst this

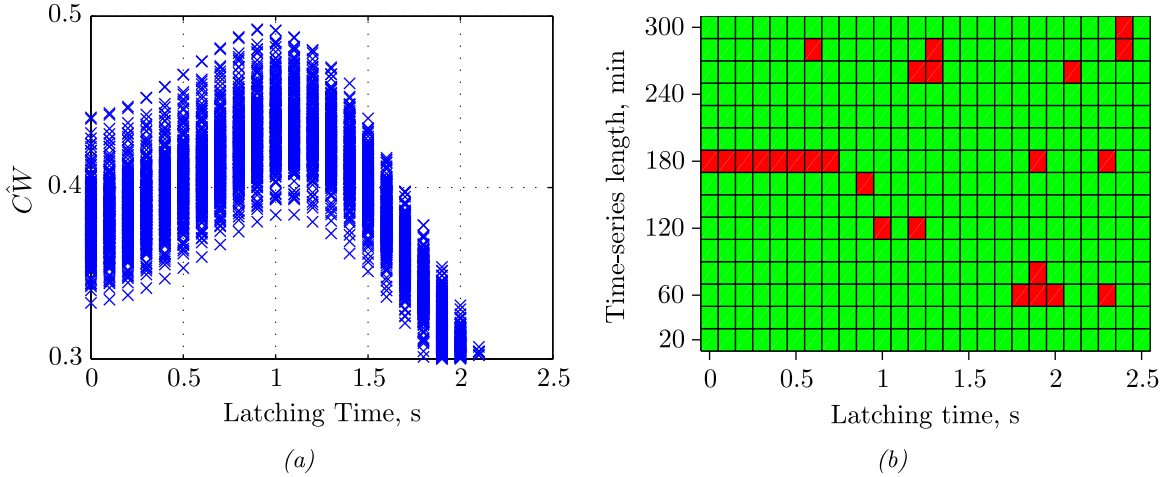

Fig. 4. (a) Monte-Carlo results of capture width estimate vs. latching time for 20 min wave time-series, and (b) Chi-Square goodness-of-fit results for Gaussian behaviour of $\hat{CW}$. In (b), rejection of the hypothesis that $\hat{CW}$ is Gaussian is indicated by red, and failure to reject the hypothesis at the $\alpha = 0.05$ significance level is indicated by green. Results for OWC in 50th percentile sea state. (For interpretation of the references to color in this figure legend, the reader is referred to the web version of this article.)

is technically not the true mean of $\hat{CW}$, which can never be determined as doing so would require an infinite time-series, the standard deviation, or random error, in CW obtained by this method was less that 0.01%, which is sufficiently small. Similarly, the true variance ${\sigma_{CW}}^2$ of $\hat{CW}$ can never be determined. Instead, a sample variance ${\sigma_s}^2$ for each latching time is determined, from which confidence bounds for ${\sigma_{CW}}^2$ can be found for each latching time. As $\hat{CW}$ is Gaussian, the sample variance ${\sigma_s}^2$ determined from N independent estimates is a Chi-Square variable (Bendat and Piersol, 2010, p. 86). Confidence bounds for ${\sigma_{CW}}^2$ are then given by

$$\text{Prob}\left(\frac{n\sigma_s^2}{\chi^2_{n;\alpha/2}} \le \sigma_{CW}^2 < \frac{n\sigma_s^2}{\chi^2_{n;1-\alpha/2}}\right) = 1-\alpha \tag{5.2}$$

where $\chi^2_{n;\alpha/2}$ is the Chi-square variable with $n = N-1$ degrees of freedom and significance level α and Prob indicates probability. Considering $\alpha = 0.05$ and $N=250$

$$0.8452\sigma_s^2 \le \sigma_{CW}^2 < 1.2018\sigma_s^2 \tag{5.3}$$

where the maximum variance $\sigma_{CW}^2 = 1.2018\sigma_s^2$ has been used in this work to produce conservative estimates for the confidence intervals for CW. Expressing $\hat{CW}$ in terms of the standard Gaussian variable z,

$$\hat{CW} = CW + z\sigma_{CW} \tag{5.4}$$

and adopting the standard definition $z_\alpha \equiv \text{Prob}(z < z_\alpha) = 1-\alpha$, 95% confidence intervals for CW can be determined for each discrete latching time

$$\text{Prob}\left(z_{\alpha/2} < \frac{\hat{CW}-CW}{\sigma_{CW}} \le z_{1-\alpha/2}\right) = 1-\alpha$$

$$\hat{CW} - 1.96\sqrt{1.2018\sigma_s^2} \le CW < \hat{CW} + 1.96\sqrt{1.2018\sigma_s^2}. \tag{5.5}$$

Confidence interval bounds for CW for the 10th, 50th and 90th percentile sea states are displayed in Fig. 5 considering time-series lengths of 20 min, 1 h, 2 h and 3 h. Confidence intervals for CW indicate the limit to which capture width can be known, and hence optimised, based on the amount of time-series information available. The optimal condition for the WEC is therefore not a single point, but a region defined by the amount of capture width information available. Any capture width within this region is optimal, with a significance level α, considering the certainty (the confidence intervals) with which the optimal capture width can be known.

5.2. Optimisation bounds for latching time

The confidence intervals for optimal capture width can be used to define optimisation bounds for the optimal mean latching time, which are bounds within which the optimal mean latching time is known to exist. The optimisation bounds are the latching times for which the mean capture width CW is equal to the lower confidence bound for CW_{opt}, being the latching times which solve

$$CW(T_L) = CW_{opt} - 1.96\sqrt{1.2018\sigma_s^2}. \tag{5.6}$$

Any latching time within this interval will yield mean capture width for the sea state CW within the confidence interval for $CW_{opt} = \max(CW)$, which, as discussed in Section 5.1, is optimal based on the capture width information available. Latching time optimisation bounds for the 10th, 50th and 90th percentile sea states are shown in Fig. 5 considering various time-series lengths. Linear interpolation was used to find the latching time bounds occurring between integer multiples of 0.1 s.

Optimisation bounds for optimal latching time vs. time-series length are shown in Fig. 6 for the 10th, 50th and 90th percentile sea states. The optimisation bounds for each sea state overlap for estimates obtained from wave time-series shorter than approximately 94 min. This means that, for sea states which are stationary for less than 94 min, there exists a set of latching times which are optimal for all sea states between the 10th and 90th percentiles. At time-series length of 94 min the bounds of the 10th and 90th percentile sea states intersect, at which point the set of optimal latching times common to all sea states is reduced to the single latching time of 1.08 s. Consequently, a fixed latching time of 1.08 s is optimal across the set of sea states between the 10th and 90th percentiles for sea states stationary for less than 94 min.

5.3. MPPT/MCWT control simulations

Simulations were performed for the MPPT and MCWT latching controlled OWC in irregular waves considering both stationary and transitioning sea states. Irregular wave time-series were produced

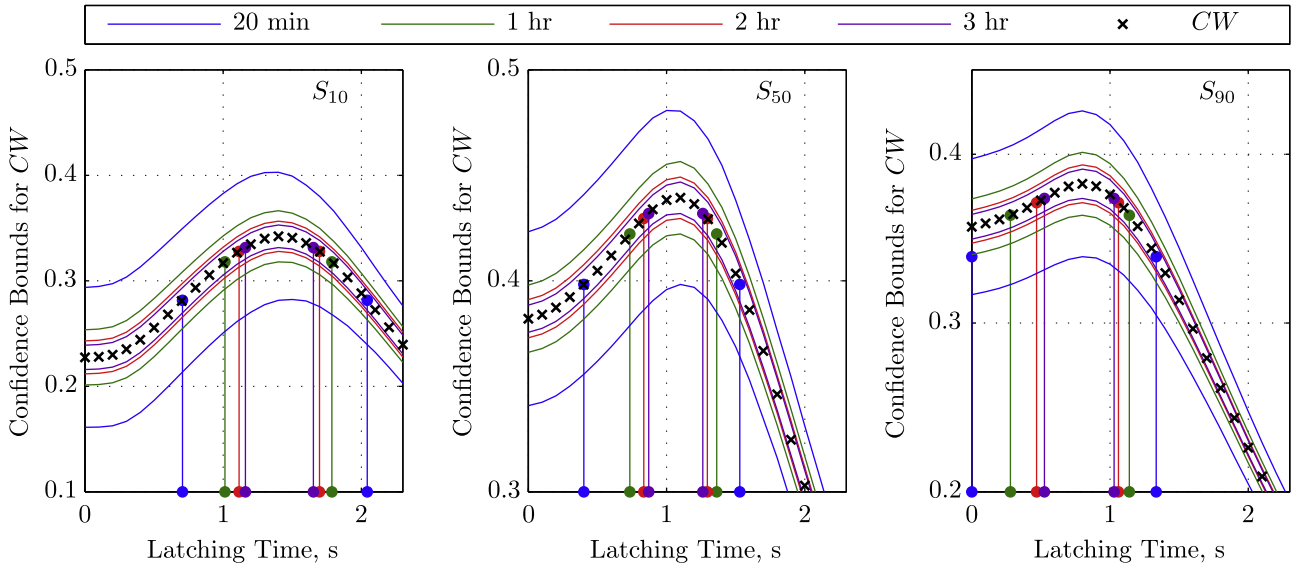

Fig. 5. Confidence intervals for mean capture width vs. latching time and corresponding optimisation bounds for latching time (vertical lines) for various wave time-series lengths for OWC in 10th (left), 50th (centre) and 90th (right) percentile sea states.

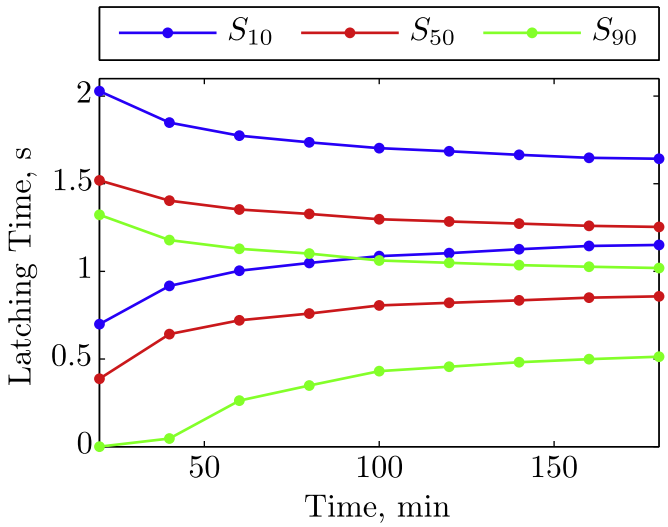

Fig. 6. Optimisation bounds for latching time vs. time-series length for various sea states.

as the weighted sum of waves generated from both 10th and 90th percentile sea states, S_{10} and S_{90} respectively, with the instantaneous sea state given by $S(t) = \big(1 - \alpha(t)\big)S_{10} + \alpha(t)S_{90}$ where $\alpha(t) \in \big[0, 1\big]$, similar to the method used in Hals et al. (2011). Stationary sea states S_{10} and S_{90} were simulated by setting $\alpha(t)$ to 0 or 1 respectively. Sea state transitions $S_{10/90}$ and $S_{90/10}$, where the subscript indicates initial/final states of transition, were modelled by ramping $\alpha(t)$ linearly over time from 0 to 1 and vice-versa. The progression of sea states in the simulations can be summarised as S_{10}, $S_{10/90}$, S_{90}, $S_{90/10}$, S_{10}, $S_{10/90}$, and S_{90}, with simulations performed for sea state durations/transitions of 3 h and 12 h. In sea states of short (3 h) duration, the MPPT and MCWT controllers were tested with update periods of 19.2 min and 59.7 min, corresponding to 18 and 56 discrete wave power estimates respectively, which are obtained via FFT every 64 s. In sea states of long (12 h) duration, controllers were tested with update periods of 19.2 min, 59.7 min, and 119.5 min, corresponding to 18, 56 and 112 discrete wave power estimates respectively. The MPPT/MCWT controllers were tested with latching time step sizes μ of 0.1 s, 0.2 s, 0.5 s, 0.7 s and 1 s. Controllers were initialised with a latching time of 1.46 s for all cases, starting in the middle of the optimisation bounds for S_{10}. Simulations were performed for 10 different irregular wave time-series for sea states S_{10} and S_{90}.

5.3.1. Time-series analysis

Time-series results for the MPPT/MCWT controllers are shown in Figs. 7 and 8 for sea states of 3 h and 12 h duration respectively. The latching time optimisation bounds and confidence intervals for optimal capture width, determined in Section 5.1, are displayed for the stationary sea states S_{10} and S_{90}.

In stationary seas, both the MPPT and MCWT controllers drive and maintain the latching time to within the optimisation bounds, with latching time being maintained within narrower optimisation bounds for increased update period, as evident in Fig. 8. Consequently, capture width is typically maintained within the 95% confidence intervals for optimal, with less variance in capture width for increased update period. Occasions exist where latching time exits the optimisation bounds, however, this is typically corrected in the next control decision. These results indicate that in stationary seas, both the MPPT and MCWT controllers can optimise OWC capture width to within the confidence bounds for which the optimal condition can be known. This result has been observed across all simulations.

In non-stationary transitioning seas, confidence intervals for the optimal capture width, and hence desired controller behaviour, are unknown. However, for seas transitioning between known states S_{10} and S_{90}, it is reasonable to assume that the latching time should be maintained between the upper and lower optimisation bounds for S_{10} and S_{90} respectively. From Figs. 7 and 8 it is evident that latching times for the MCWT controller are typically maintained between these bounds, however, latching times for the MPPT controller are not.

During sea state transitions with increasing wave power, $S_{10/90}$, MPPT can erroneously drive the latching time uni-directionally, where erroneous behaviour is qualified here as uni-directional latching time change accompanied by decreasing capture width, as shown in Figs. 7a, b and 8b. Typically, when this occurs during the $S_{10/90}$ transition, latching time is increased and driven away from the optimisation bounds of S_{90}, as in Fig. 8b. This occurs when the increasing wave power causes OWC power to increase regardless of MPPT action, causing the sign of μ in Eq. (3.1) to remain constant. In this situation latching time continues to change uni-directionally until OWC power decreases, which can be either due to system efficiency being reduced to the point where OWC power decreases despite increasing wave power, or high power variation/low system sensitivity, where the variation in OWC power due to the randomness of the irregular wave time-series is greater than the change in power due to a step change in latching time, as discussed in Ding et al. (2015). Uni-directional latching time change does not occur for the MPPT controller with fast update rate in slow transitioning seas, as shown in Fig. 8a, as the power change due to MPPT exceeds that due to the environment. Uni-directional behaviour is also less prominent for moderate μ of 0.5 s in Fig. 7c, as the larger step size increases the power change due to MPPT. MCWT occasionally exhibits "erroneous" uni-directional latching time change in increasing seas, which is not apparent in the time-series results presented, with latching time being increased beyond the upper bound for S_{10}. However, capture width continues to increase during these periods, hence the control action cannot be described as erroneous, particularly as desired controller behaviour during transitions is unknown. This behaviour is infrequent for MCWT, occurring occasionally for controllers with low μ and long update period relative to the rate of sea state transition.

During sea state transitions with decreasing wave power, $S_{90/10}$, MPPT exhibits dither, evident in Figs. 7a, b and 8b, where the latching time direction is continually reversed. Dither occurs when the magnitude of the decrease in power due to the changing environment exceeds the change in power due to the change in latching time. In this situation, OWC power continues to decrease regardless of MPPT action, causing the sign of μ in Eq. (3.1) to change every update. Dither is not evident for the MPPT controller in Fig. 8a as the short update period ensures the power change due to MPPT exceeds the power change due to the environment, and is less evident for the controller in Fig. 7c as increased μ increases power change due to MPPT. MCWT exhibits dither when the magnitude of the capture width decrease due to the environment is greater than the change in capture width due to the change in latching time, evident in Fig. 7a. MCWT is less prone to dither than MPPT as capture width is less sensitive to sea state changes than OWC power. Dither, as well as uni-directional control variable changes, occur for MCWT due to WEC being non-linear, as a change in wave power does not exactly correlate with the resulting change in capture width. However, even for this highly non-linear WEC, MCWT dither is rare and easily mitigated by a slight increase in μ, much more readily so than for MPPT.

In irregular waves the mean OWC power/capture width estimate used for decision making by the MPPT/MCWT controllers can

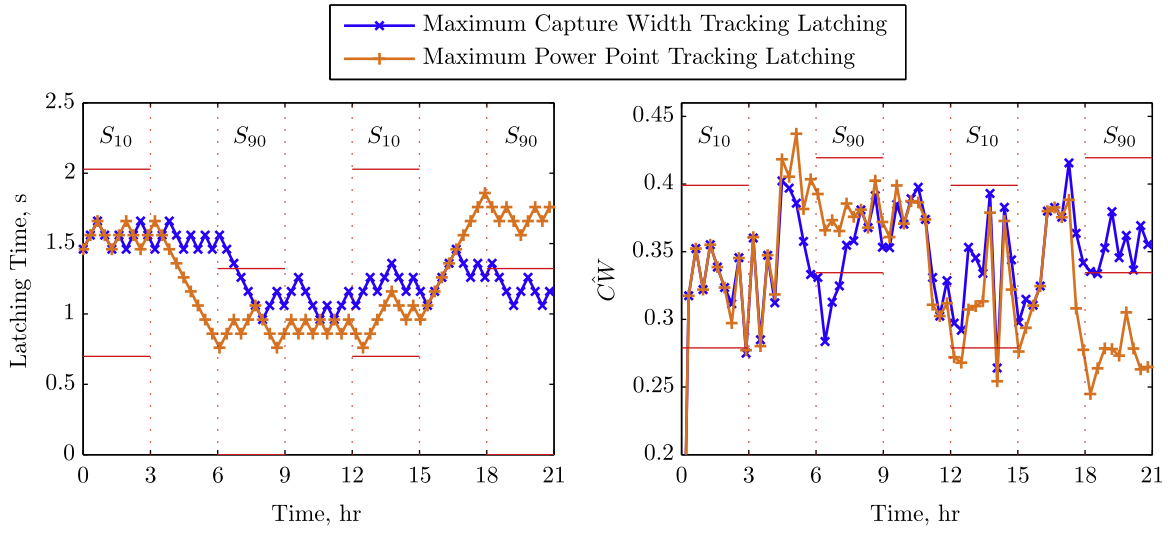

(a) μ 0.1 s, update period 19.2 min

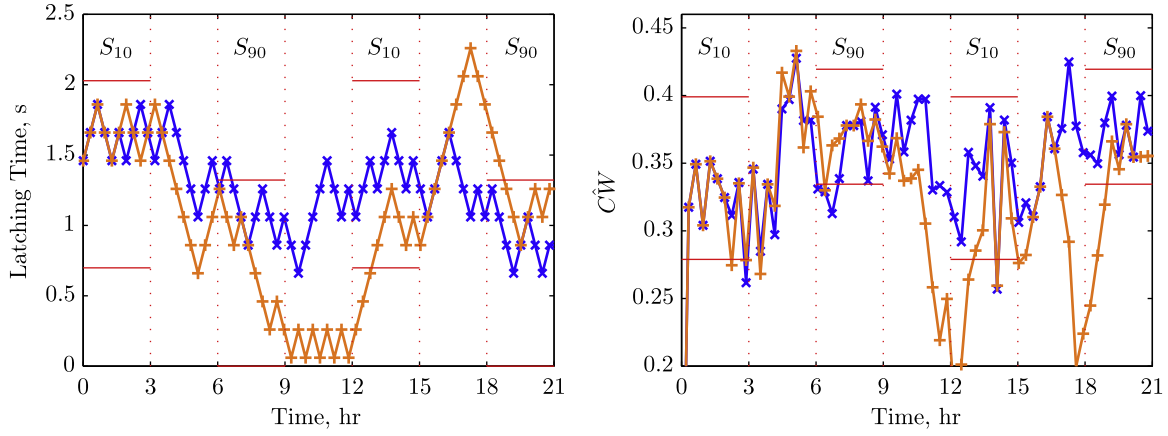

(b) μ 0.2 s, update period 19.2 min

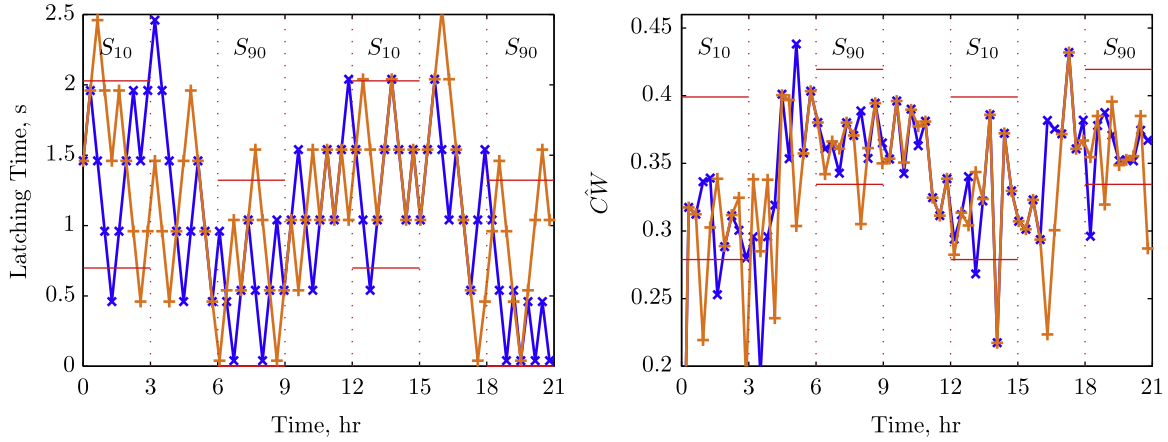

(c) μ 0.5 s, update period 19.2 min

Fig. 7. Latching time (left) and corresponding capture width (right) for MCWT and MPPT latching controllers in stationary and transitioning seas of 3 h duration. Confidence intervals for stationary sea states indicated by horizontal lines.

be regarded as a signal corrupted by a disturbance. Considering only MCWT for brevity, although similar arguments can be applied to MPPT by replacing capture width with power, the signal is the change in mean capture width due to a change in latching time, $\Delta CW(LT,\ \mu)$, where Δ is the difference operator; $\Delta x = x_k - x_{k-1}$. The disturbance contains two elements; the change in mean capture width due to a change in wave environment, $\Delta CW(J)$, and a stochastic element $\Delta\epsilon$, which can be found from Eq. (5.4) as $\Delta\epsilon = \Delta(z_k\sigma_{CW})$. Combining the signal and the disturbance yields

$$\Delta\hat{CW} = \Delta CW\left(LT,\ \mu\right) + \left[\Delta CW(J) + \Delta\epsilon\right]. \tag{5.7}$$

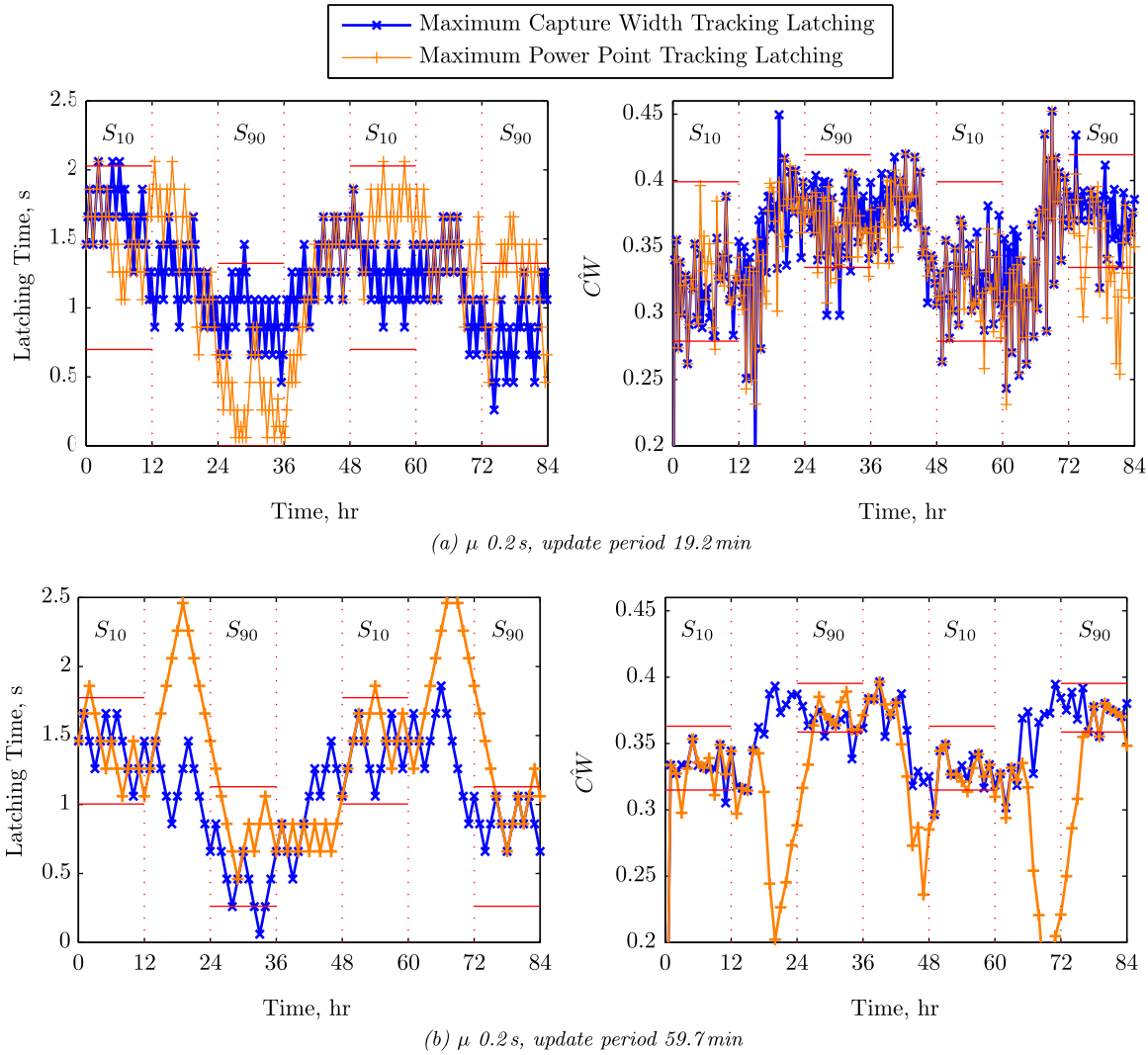

Fig. 8. Latching time (left) and corresponding capture width (right) for MCWT and MPPT latching controllers in stationary and transitioning seas of 12 h duration. Confidence intervals for stationary sea states indicated by horizontal lines.

When the magnitude of the signal, which can be increased by increasing μ, is greater than the magnitude of the disturbance, MCWT control is effective. Consequently,

$$\mathrm{sgn}\left(\Delta\hat{CW}\right) = \mathrm{sgn}\left(\Delta CW(LT,\ \mu)\right) \tag{5.8}$$

meaning that the MCWT controller, given in Eq. (3.2), acts to maximise the mean capture width. For stationary seas, MCWT maximises mean capture width by maintaining latching times within the optimisation bounds. When the disturbance magnitude is greater than the signal magnitude MCWT can be ineffective, with subsequent behaviour depending on the disturbance. If $\left|\Delta CW(J)\right| > \left|\Delta\epsilon\right|$,

$$\mathrm{sgn}\left(\Delta\hat{CW}\right) = \mathrm{sgn}\left(\Delta CW(J)\right) \tag{5.9}$$

which causes MCWT to exhibit either unidirectional latching time change or dither depending on whether seas are increasing or decreasing respectively, both of which are typical behaviour of gradient-ascent controllers in a non-stationary environment (Abdullah et al., 2012; Kazmi et al., 2010, 2011). Alternatively, if $\left|\Delta\epsilon\right| > \left|\Delta CW(J)\right|$,

$$\mathrm{sgn}\left(\Delta\hat{CW}\right) = \mathrm{sgn}(\Delta\epsilon) \tag{5.10}$$

which causes MCWT to adjust the latching time randomly as the capture width estimate varies randomly due to the irregular wave time-series. The magnitudes of both $\Delta CW(J)$ and $\Delta\epsilon$ can be influenced by the controller update period. Decreasing the update period reduces the amount of change that can occur in the environment between updates, whilst simultaneously increasing the variance of the capture width estimate, and vice versa. Consequently, controllers with short update periods are more likely to exhibit random behaviour during transitions, evident in Fig. 8a, whereas controllers with long update periods are more likely to be environment controlled during transitions, as in Fig. 8b.

5.3.2. Mean capture width

Mean capture width results were obtained for the uncontrolled system, MPPT/MCWT latching controllers, and a fixed latching time of 1.08 s, which are shown in Figs. 9a and b for sea states of 3 h and 12 h duration respectively. For each of the 10 different time-series considered, the mean capture width over the simulation time, $\hat{CW}_{mean}$, was determined, yielding 10 unique $\hat{CW}_{mean}$ values for each controller/update period combination. The results in Fig. 9 indicate the mean and standard deviation of the 10 $\hat{CW}_{mean}$

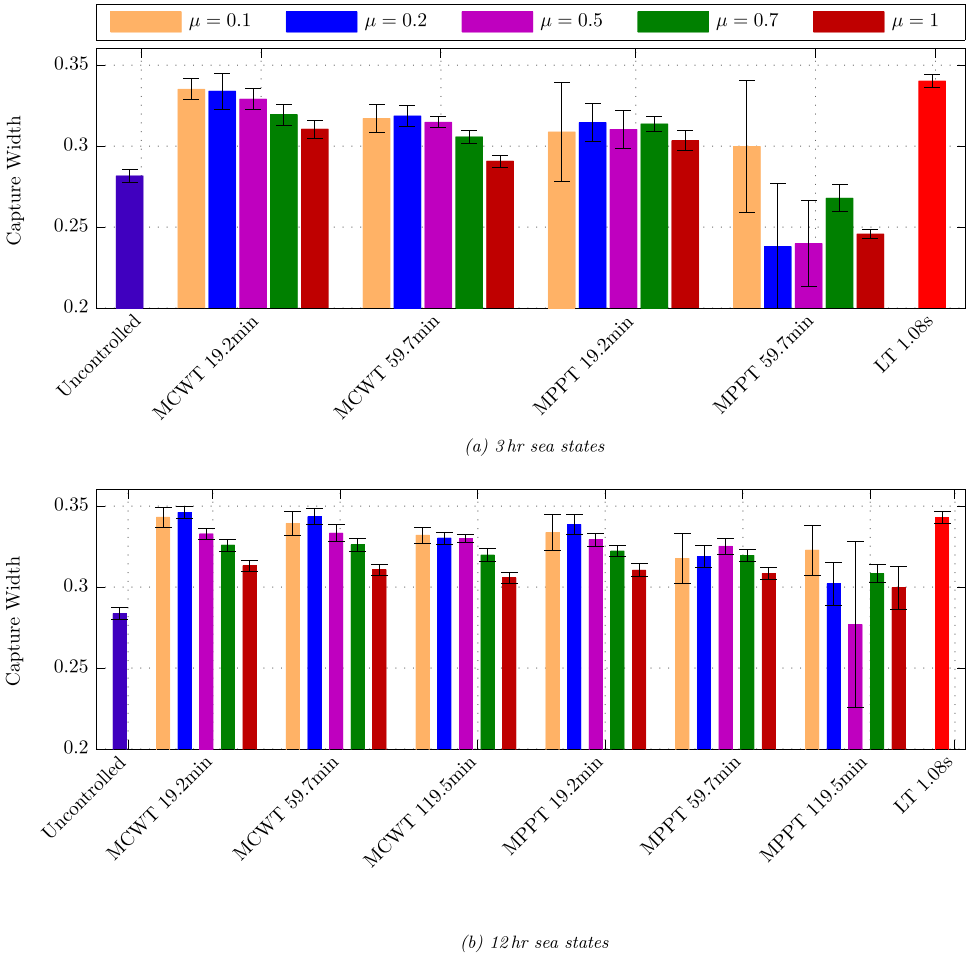

Fig. 9. Mean capture width (bars) and standard deviation (error bars) for each controller in stationary/transitioning sea states.

values for each combination.

For sea states of 3 h duration/transition the fixed latching time was found to perform best, yielding capture width of 0.340, an improvement of 21% compared to the 0.282 capture width produced by the uncontrolled system. The MCWT latching controller with update period 19.2 min performs nearly as well for μ 0.1 s or μ 0.2 s, yielding capture widths of 0.335 and 0.334 respectively. In comparison, the best performing MPPT controller for 3 h sea states, with update rate 19.2 min and μ 0.2 s, produces capture width of 0.315, a 12% improvement over the uncontrolled system. For 12 h sea states, the fixed latching time produces mean capture width of 0.343, again improving performance by 21% compared to the 0.284 capture width produced by the uncontrolled system. The best performing MCWT controllers, with update period 19.2 min and μ 0.1 s or μ 0.2 s, produce capture widths of 0.343 and 0.346 respectively, performing just as well as the fixed latching time. In comparison the best performing MPPT controllers, with update period 19.2 min and μ 0.1 s and μ 0.2 s, produce capture widths of 0.339 and 0.334 respectively, a performance improvement of approximately 19% in both cases.

The standard deviation of the mean capture width estimates indicates the degree to which controller performance is affected by the time-series representation of a sea state. A large standard deviation indicates that controller performance is more dependent on the time-series representation of the sea state rather than the sea state itself, whereas a low standard deviation indicates that the controller will perform consistently in a sea state regardless of the wave time-series. Standard deviations for the MCWT controllers are similar in all cases and comparable to standard deviations for the uncontrolled system and fixed latching time, indicating controller robustness and reliability. This means that the performance of an MCWT controller in one time-series representation of a sea state is likely a good indicator of performance across all time-series representations of the sea state.

Standard deviations for MPPT vary significantly. For the MPPT controllers updating at 19.2 min in 3 h sea states, and 19.2 min and 59.7 min in 12 h sea states, standard deviation increases for decreasing μ. Decreasing μ decreases the magnitude of the MPPT signal, increasing the likelihood that the controller will make decisions based on the disturbance. Additionally, for the latter controllers in 12 h seas, decreasing the update period from 59.7 min to 19.2 min yields a slight decrease in standard deviation across all μ. Decreasing the update period increases the likelihood that $|\Delta\epsilon| > |\Delta CW(J)|$, meaning the controller will adjust the latching time randomly during sea state transitions due to the randomness in the power estimate. This can be beneficial for MPPT in increasing seas as the latching time is unlikely to be driven too far from optimal, which can occur for uni-directional latching time changes, as in Fig. 8b. Hence MPPT standard deviations increasing with smaller μ and longer update period are reasonable. This also explains why, for MPPT in 12 h seas, the best performing μ increases from 0.2 s to 0.5 s as update period increases from 19.2 min to 59.7 min, since increasing μ acts to increase the signal magnitude, which counteracts the increased environmental power change with longer update period. Significant variations in mean capture width and standard deviation occur across the range of μ for MPPT controllers updating at 59.7 min in 3 h sea states and 119.5 min in 12 h sea states, indicating unreliability and lack

robustness to a changing environment.

Mean capture width vs. μ is a concave function for the MCWT controllers, with peak capture width typically occurring for μ of approximately 0.2 s. This result is also observable for MPPT, however, it does not apply to all controllers, occurring only for those in 12 h seas updating at 19.2 min and 59.7 min. In stationary seas, latching time variations inside the optimal region can be quite random, hence increasing μ tends to increase the occurrence of latching times exceeding the optimisation bounds, evident in Fig. 7, causing capture width to decrease. Conversely, in transitioning seas, decreasing μ reduces the signal magnitude, increasing the likelihood of the MPPT/MCWT controllers making decisions based on the disturbance. It therefore seems reasonable that, for a well-behaving controller with fixed update period, a single μ would exist that is optimal for the set of sea states considered.

5.4. MCWT improvements over fixed latching time

The simulation results of Section 5.3 indicate that MCWT latching control can produce comparable performance to that of the system with a fixed latching time optimised across the expected sea states. However, the MCWT controller requires sensors to measure wave amplitudes and WEC power whereas the fixed latching time does not, meaning MCWT control will be more expensive to implement in real life. This then raises the question of why use an adaptive controller at all when a fixed latching time performs just as well? Implementing a fixed latching time is an open-loop approach reliant on assumptions, whereas MCWT control uses measurements of physical quantities. Determining the fixed latching time in this work required the assumption that sea spectra were fully developed, stationary, and uni-modal. Applying the fixed latching time controller to a physical system would require the assumption that the model used to develop the controller is an adequate representation of the physical system. Alternatively, extensive experimental testing could be performed to determine the latching time vs. capture width characteristic for the physical system in stochastic waves, however, this still requires assumptions regarding the nature of sea states. Furthermore, system dynamics can change, either over short time-scales, such as water depth changes with tide which can affect WEC dynamics (specifically for a fixed OWC) and incoming wave profiles, or over longer time-scales, such as components aging and wearing. Whilst the fixed latching time may perform well in simulations, performance in reality can only be guaranteed as far as the model assumptions are valid. In contrast, MCWT control acts on measured data and requires no assumptions or mathematical model. The only requirement for MCWT is that the system have a smooth capture width vs. control variable characteristic with a single maxima.

5.5. OWC response in bi-modal spectra

The simulation results presented in Section 5.3 showed that for uni-modal, stationary wave systems, MCWT latching control can optimise capture width to within the confidence bounds that optimal capture width can be known. Real ocean waves, however, are not always uni-modal. Bi-modal waves can occur when low frequency swell from a distant wave system merges with local wind waves, yielding a wave system with two spectral peaks (Guedes Soares, 1984). It is well known that the performance of gradient ascent algorithms can be inhibited by the presence of local maxima in the control surface as the algorithms can track the sub-optimal peaks instead of the global optimum. This section will provide a brief investigation into the capture width vs. latching time characteristics of an OWC in bi-modal waves, specifically to determine whether or not the OWC response is characterised by both local and global maxima.

Simulations were performed for the OWC in bi-modal waves to determine the capture width vs. latching time characteristic. Bi-modal spectra were created (Guedes Soares, 1984), where separate wind wave and swell spectra, S_w and S_s respectively, are generated and summed to produce the resulting bi-modal spectra, $S_b = S_s + S_w$. Wind waves and swell were modelled using modified ISSC spectra, being fully-developed spectra modified by the inclusion of a spectral peak sharpness factor to allow for modelling of both fully developed and fetch-limited (developing) waves. The individual swell and wind wave spectra, and consequently the bi-modal spectra, are defined by 5 independent variables; the desired significant wave height of the bi-modal spectra H_b, the desired mean spectral period T_b, the significant wave height ratio of swell to wind waves $H_R = H_s/H_w$, the peak period ratio of swell to wind waves $T_R = T_s/T_w$, and the sharpness factor γ. The mean spectral period T_b was set to 8 s for all simulations. The sharpness factor γ was set to 6, indicating sharp-peaked spectra characteristic of fetch limited waves, to accentuate separation of the modal peaks of the combined spectra. Simulations were performed for bi-modal spectra with significant wave heights H_b of 1 m, 2 m and 3 m, peak period ratios T_R of 1.25, 1.5 and 1.75, and significant wave height ratios H_R of 0.5, 0.75, 1, 1.25 and 1.5, yielding a total of 45 simulation runs. Similar to the simulations performed in Sections 5.1 and 5.3, wave time-series were generated using 1000 discrete randomised frequencies with random phase.

Results of capture width vs. latching time for bi-modal spectra are displayed in Fig. 10 where only the results for T_R of 1.75 have been included for brevity. Negative capture width occurs for low wave amplitudes as the viscous losses of the turbine, which is operating at constant speed, exceed the power extracted from the waves. The results in Fig. 10 indicate that the capture width vs. latching time characteristics have single maxima for bi-modal waves, a result which was repeated across all 45 simulations. It is possible that secondary, suboptimal capture width peaks exist at longer latching times than those considered, however, the effect of these suboptimal peaks on MCWT effectiveness can be mitigated by placing an upper limit on the feasible latching times. In this case a limit of 5 s would be sufficient, and generous considering optimal latching times for the 10th, 50th and 90th percentile sea states for South Australian waters all occur for latching times shorter than 2 s. In conclusion, the simulation results indicate that MCWT latching control will work effectively in bi-modal waves.

6. Conclusion

This work presented a maximum capture width (MCWT) tracking latching controller for an OWC and investigated controller performance in irregular waves. Monte-Carlo simulations of an OWC in stationary seas showed that capture width can be approximated as a Gaussian random variable, and hence confidence intervals for mean capture width can be defined. Capture width confidence intervals were derived for the OWC considered for several South Australian sea states, allowing for subsequent definition of latching time optimisation bounds. It was shown that the optimal condition for a WEC is not a single point, but a region defined by the amount of capture width information available. Investigation of the latching time optimisation bounds showed that, for South Australian sea states stationary for less than 94 min, a set of fixed latching times exist which are optimal across all sea states between the 10th and 90th percentiles.

MPPT/MCWT latching control simulations were performed for stationary and transitioning sea states. The simulations results showed that in stationary sea states both MPPT and MCWT controllers can optimise a WEC to within the confidence bounds that

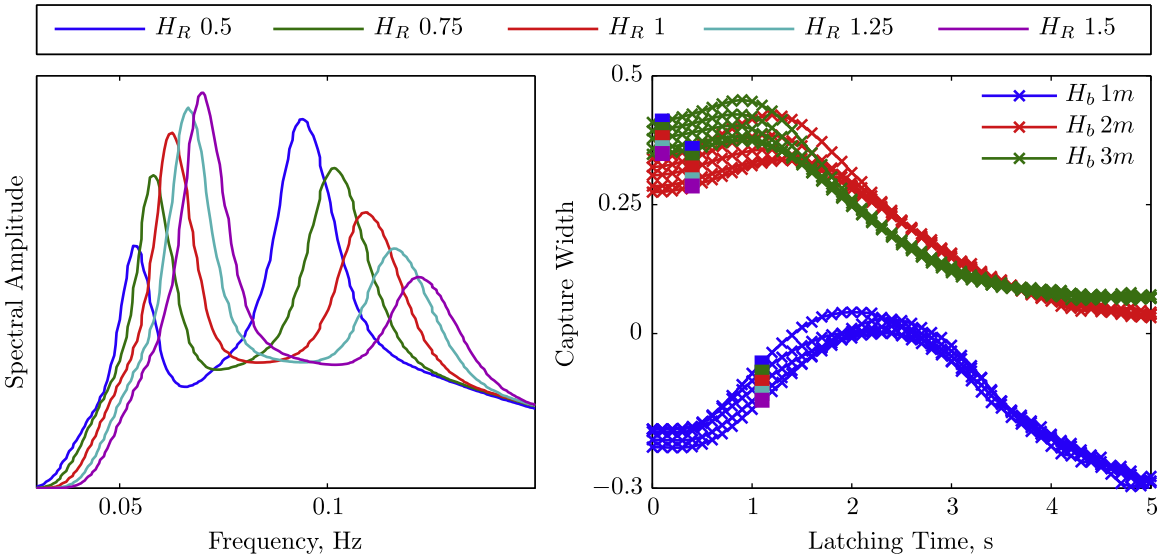

Fig. 10. Bi-modal spectra of various shape defined by significant wave height ratio H_R (left) and capture width vs. latching time for each bi-modal shape with increasing significant wave height/spectral amplitude H_b (right), where marker color indicates the bi-modal spectra shape defined by H_R, and line color indicates the significant wave height of the spectra H_b. Peak period ratio of swell to wind waves T_R is 1.75 for all cases. (For interpretation of the references to color in this figure legend, the reader is referred to the web version of this article.)

optimal capture width can be known. In transitioning sea states MCWT control was found to be robust to the changing environment, whereas MPPT control was not. MCWT control was found to be capable of producing capture width equivalent to that of a fixed latching time optimised across the range of sea states. Additionally, it was found that a short controller update period is desirable, which reduces lag, despite reduced controller convergence due to increased confidence intervals for optimal capture width. For a real life WEC, the update period should be selected based on the stationarity of the sea states at the WEC site, where a short update period would be appropriate for a site with high variability, and a longer period applicable for steadier, more stationary sites. Finally, a brief investigation into OWC performance in bi-modal seas was conducted, where it was found that the capture width vs. latching time characteristics of the OWC were smooth with single maxima, indicating MCWT latching control will be effective in multi-modal seas.

Acknowledgments

Peter Hardy would like to thank the Playford Trust, South Australia, for financial assistance.

References

Abdullah, M.A., Yatim, A.H.M., Tan, C.W., Saidur, R., 2012. A review of maximum power point tracking algorithms for wind energy systems. Renew. Sustain. Energy Rev. 16, 3220–3227.

Amon, E.A., Schacher, A.A., Brekken, T.K.A., 2009. A novel maximum power point tracking algorithm for ocean wave energy devices. In: Proceedings of the Energy Conversion Congress and Exposition, pp. 2635–2641.

Amon, E.A., Brekken, T.K.A., Schacher, A.A., 2012. Maximum power point tracking for ocean wave energy conversion. IEEE Trans. Ind. Appl. 48 (3), 1079–1086.

Babarit, A., Clément, A.H., 2006. Optimal latching control of a wave energy device in regular and irregular waves. Appl. Ocean Res. 28, 77–91.

Babarit, A., Duclos, G., Clément, A.H., 2004. Comparison of latching control strategies for a heaving wave energy device in random sea. Appl. Ocean Res. 26 (5), 227–238.

Babarit, A., Hals, J., Muliawan, M., Kurniawan, A., Moan, T., Krokstad, J., 2012. Numerical benchmarking study of a selection of wave energy converters. Renew. Energy 41, 44–63.

Barzilai, J., Borwein, J.M., 1988. Two-point step size gradient methods. IMA J. Numer. Anal. 8, 141–148.

Bendat, J., Piersol, A., 2010. Random Data: Analysis and Measurement Procedures, 4th ed. Wiley.

Clément, A.H., Babarit, A., 2012. Discrete control of resonant wave energy converters. Philos. Trans. R. Soc. A 370, 288–314.

Cruz, J., 2008. Ocean Wave Energy – Current Status and Future Perspectives. Springer-Verlag, Berlin.

Ding, B., Cazzolato, B., Arjomandi, M., Hardy, P., 2015. Sea-state based maximum power point tracking damping control of a fully submerged oscillating buoy. Ocean Eng., In preparation

Evans, D.V., 1982. Wave-power absorption by systems of oscillating pressure distributions. J. Fluid Mech. 114, 481–499.

Evans, D.V., Porter, R., 1995. Hydrodynamic characteristics of an oscillating water column device. Appl. Ocean Res. 17, 155–164.

Falcão, A., 2002. Control of an oscillating-water-column wave power plant for maximum energy production. Appl. Ocean Res. 24, 73–82.

Falcão, A., Justino, P.A.P., 1999. OWC wave energy devices with air flow control. Ocean Eng. 26, 1275–1295.

Falcão, A., Rodrigues, R., 2002. Stochastic modelling of OWC wave power plant performance. Appl. Ocean Res. 24, 59–71.

Falnes, J., 2002. Ocean Waves and Oscillating Systems. Cambridge University Press, UK.

Faltinsen, O.M., 1993. Sea Loads on Ships and Offshore Structures. Cambridge University Press, Cambridge, United Kingdom.

Garcia-Ross, P.B., Lizarralde, F., Estefen, S., 2012. Optimization of the wave energy absorption in oscillating-body systems using extremum seeking approach. In: Proceedings of the American Control Conference, pp. 1011–1016.

Gkikas, G.D., Athanassoulis, G.A., 2014. Development of a novel nonlinear system identification scheme for the pressure fluctuation inside an oscillating water column-wave energy converter Part I: theoretical background and harmonic excitation case. Ocean Eng. 80, 84–99.

Goda, Y., 2010. Random Seas and Design of Maritime Structures vol. third. World Scientific Publishing, Singapore.

Guedes Soares, C., 1984. Representation of double-peaked sea wave spectra. Ocean Eng. 11 (2), 185–207.

Hals, J., Falnes, J., Moan, T., 2011. A comparison of selected strategies for adaptive control of wave energy converters. J. Offshore Mech. Arct. Eng. 133 031101–1–12.

Hemer, M.A., Griffin, D.A., 2010. The wave energy resource along Australia's southern margin. J. Renew. Sustain. Energy 2 (4) 043108–1–15.

Henriques, J.C.C., Gato, L.M.C., Falcão, A., Robles, E., Faÿ, F.-X., 2016. Latching control of a floating oscillating-water-column wave energy converter. Renew. Energy 90, 229–241.

Hughes, M.G., Heap, A.D., 2010. National-scale wave energy resource assessment for Australia. Renew. Energy 35, 1783–1791.

ITTC, 2002. The specialist committee on waves, Final report and recommendations to the 23rd ITTC. In: Proceedings of the 23rd International Towing Tank Conference, vol. 2, pp. 505–551.

Jefferys, R., Whittaker, T., 1985. Latching control of an oscillating water column device with air compressibility. In: Evans, D.V., Falcáo, A. (Eds.), Hydrodynamics of Ocean Wave-Energy Utilization. Springer-Verlag, Berlin, Heidelberg, pp. 281–292.

Kazmi, S.M.R., Goto, H., Hai-Jiao, G., Ichinokura, O., 2010. Review and critical

analysis of the research papers published till date on maximum power point tracking in wind energy conversion system. In: Proceedings of the Energy Conversion Congress and Exposition, IEEE, pp. 4075–4082.
Kazmi, S.M.R., Goto, H., Hai-Jiao, G., Ichinokura, O., 2011. A novel algorithm for fast and efficient speed-sensorless maximum power point tracking in wind energy conversion system. IEEE Trans. Ind. Electron. 58 (1), 29–36.
Lattanzio, S.M., Scruggs, J.T., 2011. Maximum power generation of a wave energy converter in a stochastic environment. In: Proceedings of the IEEE International Conference on Control Applications, pp. 1125–1130.
Lopes, M.F.P., Hals, J., Gomes, R.P.F., Moan, T., Gato, L.M.C., Falcão, A., 2009. Experimental and numerical investigation of non-predictive phase-control strategies for a point-absorbing wave energy converter. Ocean Eng. 36, 386–402.
McCormick, M.C., 2010. Ocean Engineering Mechanics with Applications. Cambridge University Press, New York, USA.
Perez, T., Fossen, T.I., 2009. A Matlab toolbox for parametric identification of radiation-force models of ships and offshore structures. Model. Identif. Control 30 (1), 1–15.
Ringwood, Fusco, 2012. A study of the prediction requirements in real-time control of wave energy converters. IEEE Trans. Sustain. Energy 3 (1), 176–184.
Snyder, S.D., 2000. Active Noise Control Primer. Springer-Verlag, New York.
Taghipour, R., Perez, T., Moan, T., 2008. Hybrid frequency-time domain models for dynamic response analysis of marine structures. Appl. Ocean Res. 35, 685–705.
Welch, P., 1967. The use of fast Fourier transform for the estimation of power spectra: A method based on time averaging over short, modified periodograms. IEEE Trans. Audio Electroacoust. 15 (2), 70–73.
Yuan, Y.X., 2008. Step-sizes for the gradient method. In: Liu, K.S., Xin, Z.P., Yau, S.T. (Eds.), Third International Congress of Chinese Mathematicians (AMS/IP Studies in Advanced Mathematics), American Mathematical Society/International Press, pp. 785–796.
Yu, Z., Falnes, J., 1995. State-space modelling of a vertical cylinder in heave. Appl. Ocean Res. 17, 265–275.